Available online at www.sciencedirect.com
SCIENCE DIRECT®
Journal of Sound and Vibration 296 (2006) 676–689
JOURNAL OF SOUND AND VIBRATION
www.elsevier.com/locate/jsvi

Vibrations and stability of a flexible disk rotating in a gas-filled enclosure—Part 2: Experimental study

Namcheol Kang, Arvind Raman*

Mechanical Engineering, Purdue University, 585 Purdue Mall, West Lafayette, IN 47907-2088, USA

Received 14 December 2004; received in revised form 4 August 2005; accepted 10 September 2005
Available online 22 June 2006

Abstract

The vibrations and acoustic oscillations of a rotating disk coupled to surrounding fluids in an air-filled enclosure are investigated experimentally. Aeroelastically excited disk transverse vibrations are measured in a specially designed enclosure on a high-speed test stand using different disk materials. In addition, acoustic modes are monitored as a function of disk rotating speed using microphones which are installed at the top and bottom covers of the enclosure. It is shown from the acoustic pressure measurements that acoustic modes can be classified as in-plane modes that decouple from disk vibration or out-of-phase modes that couple to disk vibration. Further, it is also shown that with disk rotation both these types of acoustic modes split into forward and backward traveling waves, offering direct evidence of a rotating core in the fluid flow in the enclosure. It is confirmed from measurements of the disk vibration that disk flutter does not occur by mode coalescence but by a damping-induced instability as described in the accompanying theoretical paper. Beyond the flutter speed, it is shown that acoustic pressures oscillate severely at the frequency of disk instability. These phenomena are, for the most part, predicted by accompanying theory. Other phenomena are observed that are not predicted by current theory including moderate amplitude 1/2 rotation speed subharmonics in the disk vibration spectrum. Put together these experiments confirm several theoretical predictions, but also reveal new phenomena that can occur in enclosed rotating disk systems such as in CD/DVD ROMs, hard disk drives, and micro-gas turbines.

1. Introduction

The fluid–structure interactions of enclosed flexible rotating disks are important for the design of several precision electromechanical systems such as DVD ROM, hard disk drives, micro-fabricated gas turbines, etc. In the accompanying theoretical paper, the acoustic–structure interactions and aeroelastic stability of a flexible disk rotating in a fluid-filled enclosure are investigated. In this paper, we focus on new experimental investigations of this problem.

Broadly speaking the literature on experiments in fluid–structure interaction of rotating disks can be classified into three categories. In the first, the turbulence or unsteady flow-induced disk vibrations have been investigated in hard disk platters [1–3]. Turbulence-induced disk vibrations are directly correlated to track

*Corresponding author. Tel.: +1 765 494 5733; fax: +1 765 494 0539.
E-mail address: raman@ecn.purdue.edu (A. Raman).

0022-460X/$ - see front matter © 2006 Elsevier Ltd. All rights reserved.
doi:10.1016/j.jsv.2005.09.023

misregistration in hard disk drives. In their experiments Bouchard and Talke [4] found 34.5% smaller amplitude of the turbulent-excited disk vibration in helium than that in air. Moreover all these experiments were performed at disk subcritical speeds.

In the second category of problems at supercritical disk speeds, the rotating disks loose stability and start oscillating suddenly with large amplitude. This phenomenon is known as *flutter instability* and is a fluid-coupling-induced self-excited instability. D'Angelo and Mote [5] performed experimental studies at various gas densities, and first observed flutter instability at supercritical speed of a thin steel disk. Later, Renshaw et al. [6] showed experimentally that the onset of flutter instability depends on fluid density and disk rotating speed. Hansen et al. [7] proposed an experimental method for predicting the onset of flutter of a spinning disk in a fluid medium using the damping parameters of forward and backward traveling waves. Later Kim et al. [8] applied the same method to enclosed hard disk drives with varying air gaps. In spite of this experimental work, the *enclosed* rotating disk problem is poorly understood.

In the third category of experiments on disk–fluid coupling, researchers have investigated the acoustic–disk coupling. Acoustic oscillations in the enclosure can couple significantly to structural vibrations, and this can play an important role in determining the stability of the flexible disk. Tseng and Wickert [9] showed experimentally that the vibration modes in a disk stack split due to acoustic coupling between the disks. Recently, Park and Shen [10] studied acoustic–structure couplings of multiple disks by modeling the air between disks as discrete springs. According to their experimental results, the air couples the corresponding traveling waves on each disk and rearranges them into a group of traveling waves with distinct frequencies.

This study describes the experimental investigations of the vibrations and stability of a rotating disk coupled to acoustic oscillations of surrounding air in a cylindrical enclosure. Disk and acoustic pressure oscillations are measured in a specially designed enclosure on a high-speed test stand using different disk materials, and compared with theoretical predictions described in Part 1. Several experimental results agree well with the theoretical predictions, while some experimental findings are new and do not appear to be predicted by proposed theory. In what follows we will describe in sequence: (1) the experimental setup, (2) the experimental procedure, (3) experimental results and conclusions.

2. Experimental setup and procedure

2.1. Experimental setup

As shown in Fig. 1(a), a high-speed SpinStand (TTi, Inc., http://www.tti-us.com/) is placed in the safety chamber with a PC-based motor controller, which enables disk rotations up to 30,000 rev/min using a

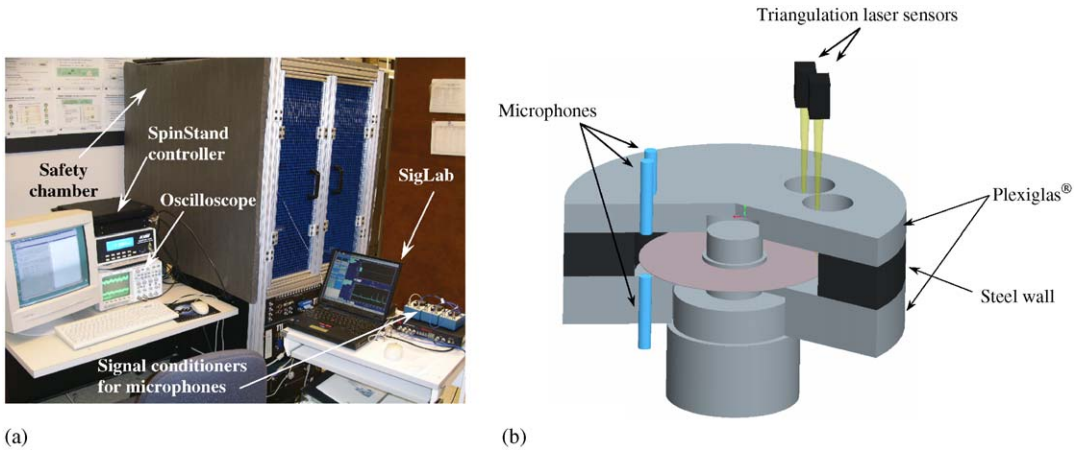

Fig. 1. A specially designed experimental setup: (a) a photograph of the experimental setup and (b) schematic diagram of measurement system.

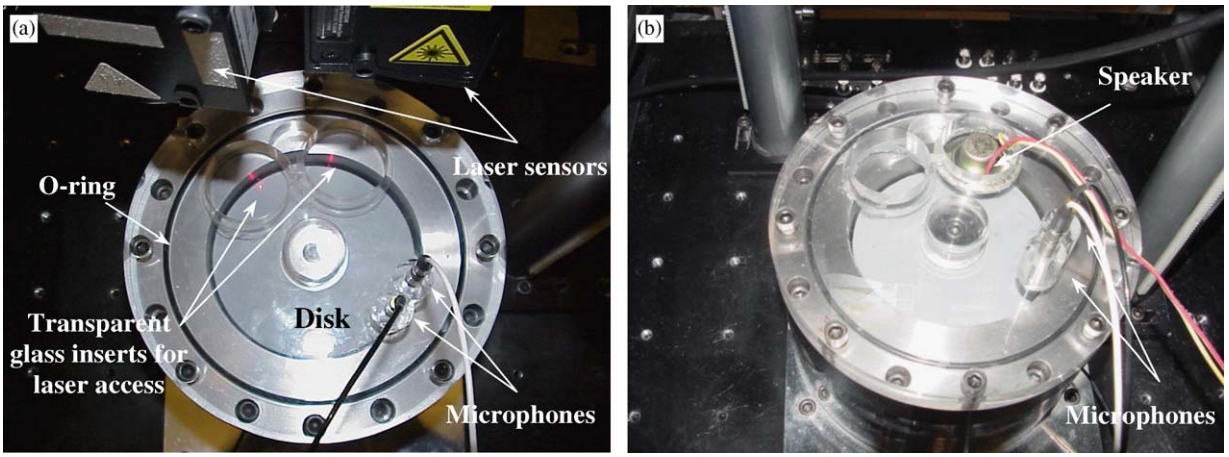

Fig. 2. Photographs of the experimental setup including the enclosure and sensors: (a) enclosure with disk, top cover, and two laser sensors and microphones and (b) top cover when a speaker is installed in the plane of a transparent glass insert. Plexiglas® acts as a material with acoustic absorption properties that are different from steel. Transparent glasses are used to allow for easy optical access for the laser sensors to measure disk vibration.

Table 1
Dimensions of the cylindrical enclosure and disk

Design parameter	Dimensions (cm)
Outer radius of enclosure	4.953
Outer radius of disk	4.750
Inner radius of disk	1.600
Radius of shaft	1.397
Distance between disk and top cover	1.397
Distance between disk and bottom cover	0.889

high-precision and low runout spindle. The spindle motor (3 phase brushless D.C., 8 pole) has an optical encoder with 4096 pulses per revolution, and the speed of it is controlled by a PID control loop through user-defined gains. In a separate experiment, the lowest natural frequency of the spindle is measured to be approximately 800 Hz, and this is much higher than the measured disk frequencies in this experiment. The software Trib98 (TTi, Inc.) is used to control the spindle speed, and the associated script language is used to completely automate the test.

A schematic diagram shown in Fig. 1(b) illustrates a specially designed enclosure and measuring sensors. The enclosure is composed of three parts with two different materials in order to provide rigid and absorbent wall conditions respectively at sidewall and top/bottom covers of the enclosure. O-rings are inserted between each component of the enclosure to prevent air leakage, and then each component is bolted tightly to the enclosure. Plexiglas® covers at the top and bottom provide different acoustic boundary conditions that are different from the steel sidewall (see Fig. 2). Plexiglas® has different acoustic absorption properties from steel[1]. Two glass inserts with high optical transparency on the top cover are used to allow easy optical access to the laser to measure disk vibration. Significant effort is made to ensure that the microphones and glass inserts sit flush with the inner surface of the enclosure. The main enclosure and disk dimensions are shown in Table 1 and depicted in Fig. 1(b).

Several sensors are used to monitor disk vibration and acoustic oscillations. Laser triangulation sensors (MTI instrument, Microtrak 7000) measure the transverse displacements of a rotating disk. Specifically, two

[1]Typically, acoustic impedance of Plexiglas and steel are 3.2×10^6 and 46.5×10^6 kg/m^2 s, respectively.

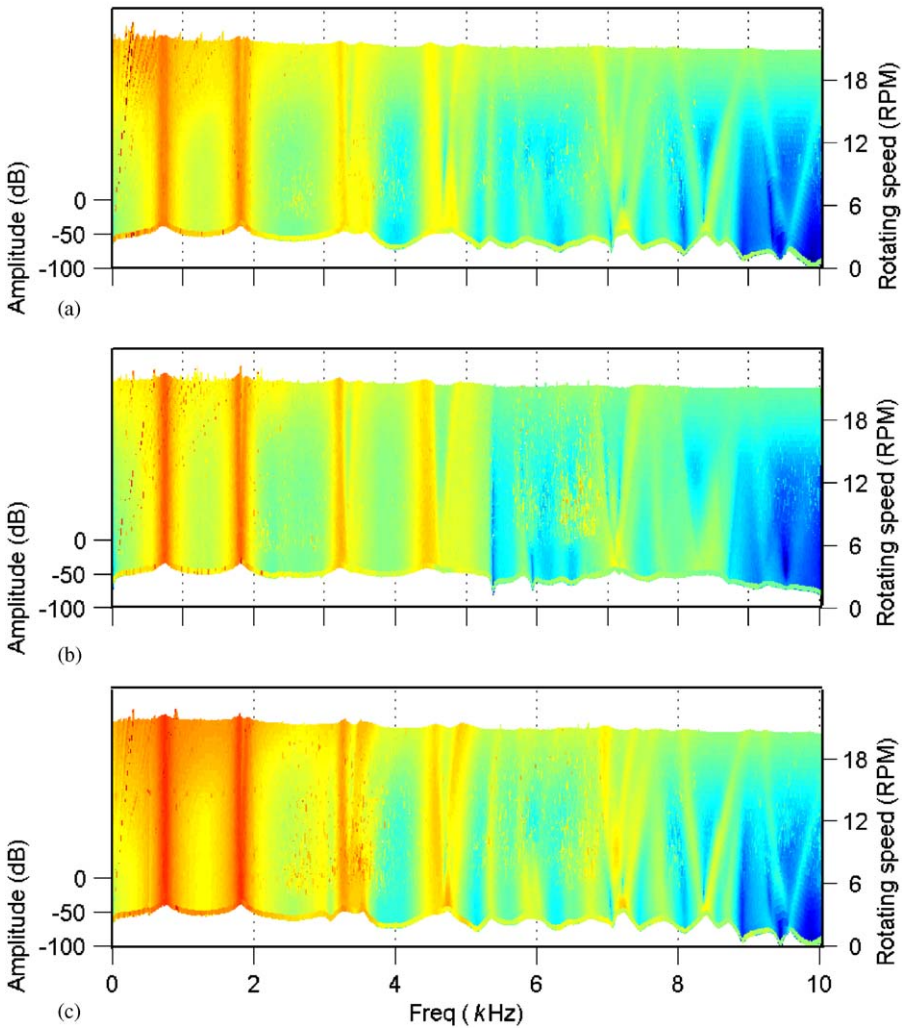

Fig. 3. Waterfall plot of acoustic pressures in the enclosure: (a) plastic disk (0.003″ thick), (b) stainless-steel disk (0.004″ thick), and (c) aluminum disk (0.005″ thick).

sensor heads are used to facilitate the identification of the nodal diameter number of the disk vibration modes. Microphones (PCB, 1/4″ Prepolarized Free-field Type 40BE) measure the acoustic pressure in the enclosure at the top and bottom covers of the wall simultaneously. Two microphones are located with a 20° angular separation at the top cover for the same reason as that for the laser sensors. Similarly, two microphones at top and bottom covers are used to identify in-phase and out-of-phase acoustic modes of the enclosure. Note that for the measurement of acoustic modes, a speaker (0.2 W, 8Ω, 45 mm in diameter) is used to apply random excitation to the acoustic cavity modes. In this case, one of transparent glass inserts is replaced with the speaker (see Fig. 3).

Three different disk materials and three different thicknesses are used for the experiments, and some of their uncoupled natural frequencies and material properties are calculated in Table 2. In order to observe flutter instability within the operating speed ranges of the SpinStand, thinner disks are chosen than those of commercial hard disk. In addition, to improve diffusive property for laser measurement, the disk are coated with spray paint (gray color). The size of the enclosure is designed to be slightly greater than that of the rotating disk (2 mm larger in radius). The corresponding uncoupled natural frequencies of the acoustic enclosure without the disk are also calculated as in Table 3.

Table 2
Uncoupled natural frequencies (Hz) of the stationary disks of different materials proposed in the experiments

Mode	Disk				
	Aluminum	Plastic			Stainless steel
(0,0)	100.83	21.11	35.19	70.37	78.15
(1,0)	100.02	20.94	34.90	69.81	77.52
(2,0)	117.20	24.54	40.90	81.80	90.84
(3,0)	183.43	38.41	64.01	128.02	142.17
(4,0)	297.71	62.33	103.89	207.78	230.75
(5,0)	449.93	94.20	157.01	314.01	348.73
Thickness (inches)	0.005	0.003	0.005	0.010	0.004
Young's modulus (Gpa)	71	4.483	4.483	4.483	195
Disk density (kg/m^3)	2700	1400	1400	1400	7900
Poisson's ratio	0.33	0.33	0.33	0.33	0.33

Dimensions of the disks except disk thickness are listed in Table 1.

Table 3
Uncoupled natural frequencies (Hz) of the acoustic enclosure

n_1	n_2			
	0	1	2	3
0	0	4223	7732	11213
1	2029	5876	9408	12902
2	3366	7391	10988	14516
3	4630	8834	12505	16076
4	5861	10231	13978	17595
5	7071	11595	15416	19082
6	8268	12934	16828	20542
7	9454	14254	18218	21979
8	10633	15558	19590	23398

n_1 and n_2 indicate the number of nodal diameter and nodal circle of the acoustic mode, respectively; z-directional acoustic modes are excluded in this calculation, because they are much higher than others.
Note: Air is used for the surrounding fluid, and its density and speed of sound are assumed as 1.2 kg/m^3 and 343 m/s, respectively.

Finally, SigLab with MATLAB is used for data acquisition and signal processing. To confirm the steady responses of the experiment, time signals are also monitored through an oscilloscope in real time.

2.2. Experimental procedures and signal processing

Several steps are taken to ensure repeatable, reliable data. Consistent clamping of the disk is one of the most important steps to ensure repeatability of the experiment [12]. In order to minimize the error caused by clamping, the disk is not disassembled until the experiment is complete. Once the disk is installed, the rotating speed of the disk is increased monotonically in small increments until the experiment is finished. At each rotating speed, a few seconds are allowed and data are acquired after this time period for the disk and airflow motions to reach steady state. The above sequential procedures are automated in Trib98. In the experiment all equipment is under room temperature without any special cooling system for the rotating disk and enclosure. Therefore, the temperature of air inside the enclosure increases somewhat due to bearing heating. However, by comparing the disk natural frequencies before and after a long period of steady operation at a fixed speed, it is determined that the effects of temperature increase induced thermal stresses are insignificant in these experiments.

Auto- and cross-power spectra are calculated from the acquired data using several ensemble averages. At each rotating speed, the experiment is performed for 5~30 min in order to achieve several hundred time averages. For example, in the case of the measurement of acoustic modes, more than 300 time averages are performed with 3.125 Hz frequency resolutions in the spectrum. At higher rotating speeds, due to the turbulence and acoustic noise from the ball bearing in spindle, signal-to-noise ratio (SNR) of the acoustic signal becomes relatively low. Consequently, this low SNR generates poor coherence between the two signals measured by the two microphones. In this study, however, the spectra are improved by averaging several times with the application of a Hanning window. For the fluid turbulence-induced disk vibration measurement, about 200 times averages with maximum overlap are performed with 0.156 Hz frequency resolutions in the spectrum.

3. Experimental results and discussions

3.1. Acoustic oscillations excited by random speaker excitation

Acoustic pressures in the cylindrical enclosure driven by the speaker are measured when the disk is rotated over a range of speeds. Auto-power spectra of the measured pressure signals are measured as a function of rotating speed to investigate the speed dependency of acoustic modes. Spectra are calculated in the 0–10 kHz frequency range, and for rotating speeds ranging from 0 to 18×10^3 rev/min with 500 rev/min speed increments. Fig. 3 illustrates waterfall plots of the acoustic pressure measured at bottom cover of the enclosure for three disks with different materials and thickness. When the disk is at rest, the coupled frequencies of all acoustic modes are close to the uncoupled natural frequencies shown in Table 3. However, as the disk rotates, each coupled acoustic mode frequency splits into two. One frequency increases with rotation speed, whereas the other decreases with rotation speed. This phenomenon occurs for all three disks, and will be investigated in detail through the observations of auto- and cross-power spectra at specific rotating speeds.

When the aluminum disk (0.005″ thick) is rotating at 500 rev/min, the auto-power spectrum of the acoustic pressure oscillations in the enclosure is shown in Fig. 4(a). The frequencies of three peaks at 1.8, 3.2, and 4.6 kHz in the auto-power spectrum are also close to the uncoupled acoustic mode frequencies as shown in Table 3. Another way to identify the acoustic modes is through the calculation of the phase angles of the cross-power spectrum measured by two microphones on the top cover (see Fig. 4(b)). According to the mode identification technique for the traveling waves of the rotating disk [13], phase angles of acoustic traveling waves are proportional to the nodal diameter number of the modes. Theoretically the phase angle is equal to the number of nodal diameter mode times the actual angle between two microphones located at the top cover with the same radii. In this experiment, however, the measured values of the phase angle are smaller than the theoretical ones. These experimental errors might be caused by phase mismatches of microphones. Nevertheless, all of them are proportional to the mode numbers and coincide well with the uncoupled acoustic modes. Note finally, the peak near 800 Hz is the natural frequency of the speaker.

In addition, the cross-spectrum between top and bottom acoustic pressure signals can be used to identify the in-phase or out-of-phase acoustic modes. For example, as shown in Fig. 4(c), all phase angles corresponding to the uncoupled acoustic modes are nearly zero. This is because acoustic modes in upper and lower cavities oscillate with the same phase. On the other hand, the phase angles corresponding to the peaks near 3.5 and 4.8 kHz are clearly non-zero. Although the measured values are not equal to the theoretical value of 180° they are far from zero and they can be identified as *out-of-phase* acoustic mode. As before, the underestimation of these values may be caused by the phase mismatch of the microphones. The acoustic pressure in the top and bottom enclosure oscillate out-of-phase and are expected to be coupled to disk vibrations.

When the disk rotates at higher speeds in the enclosure, the coupled acoustic modes show an interesting phenomenon. For instance, the auto-power spectra of acoustic pressure oscillations when the disk is rotating at 12×10^3 rev/min are illustrated in Fig. 5(a). As shown in Fig. 3, in-phase acoustic mode frequencies split into two, one higher and one lower, as the disk rotates. By observing the phase angles of the cross-power spectrum between two microphones located 20° apart on the top cover (Fig. 5(b)), it is observed that the lower frequency corresponds to an acoustic wave that travels in the opposite direction to the disk rotation (BTW),

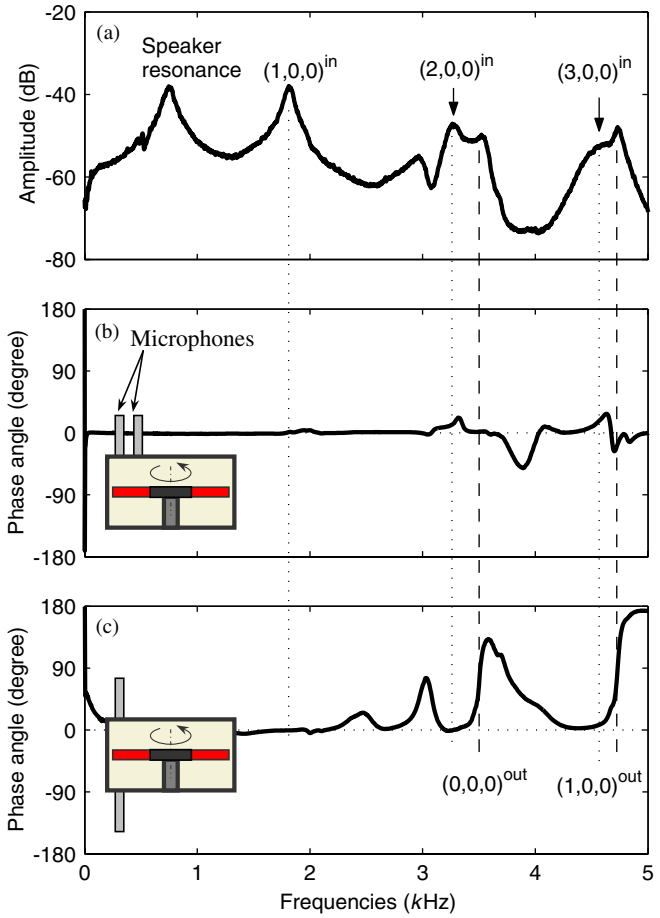

Fig. 4. Spectra of acoustic pressures oscillations in a cylindrical enclosure when aluminum disk (0.005″ thick) is rotating at 500 rev/min in the middle of the enclosure: (a) auto-power spectrum, (b) cross-power spectrum between top 1 and 2, and (c) cross-power spectrum between top and bottom.

and vice versa (FTW). This phenomenon occurs for all speed ranges, and provides direct evidence of the influence of rigidly rotating bulk fluid flow on the acoustic oscillations in the enclosure.

From the theoretical analysis in the accompanying paper [11] it is clear that the frequencies of the in-phase acoustic modes do not split if the surrounding fluid is stationary. On the other hand, it is also shown these frequencies split into forward and backward traveling waves in the presence of a bulk rotating potential core. The theory also predicts that this frequency split between the forward and backward traveling 'n' nodal diameter acoustic, in-phase modes equals $2n\Omega_f$, where Ω_f is the angular velocity of the bulk rotating core. By matching the observed frequency split of the in-phase acoustic modes, it is determined that a value of $\Omega_f \sim 30\%$ Ω_d (disk rotation speed) accurately matches the observed frequency splitting for all the disk materials tested (Fig. 3).

The above measurement of the acoustic pressures in the rotating disk–acoustic enclosure system provides substance to the assumption of rigidly rotating bulk fluid flow in the theoretical model, and will be discussed more in the next section.

The out-of-phase acoustic modes are also split into forward and backward traveling waves. However, out-of-phase acoustic modes disappear at high rotating speeds, and it is hard to identify them from the measured data in this study (see Fig. 5(c)). Physically, the out-of-phase acoustic modes have higher acoustic energy due to their spatial complexity, and therefore, greater excitation levels are required for their identification. Note that the frequency split of the out-of-phase modes occurs because of the coupling of the acoustic oscillation to the rotating disk vibrations [11].

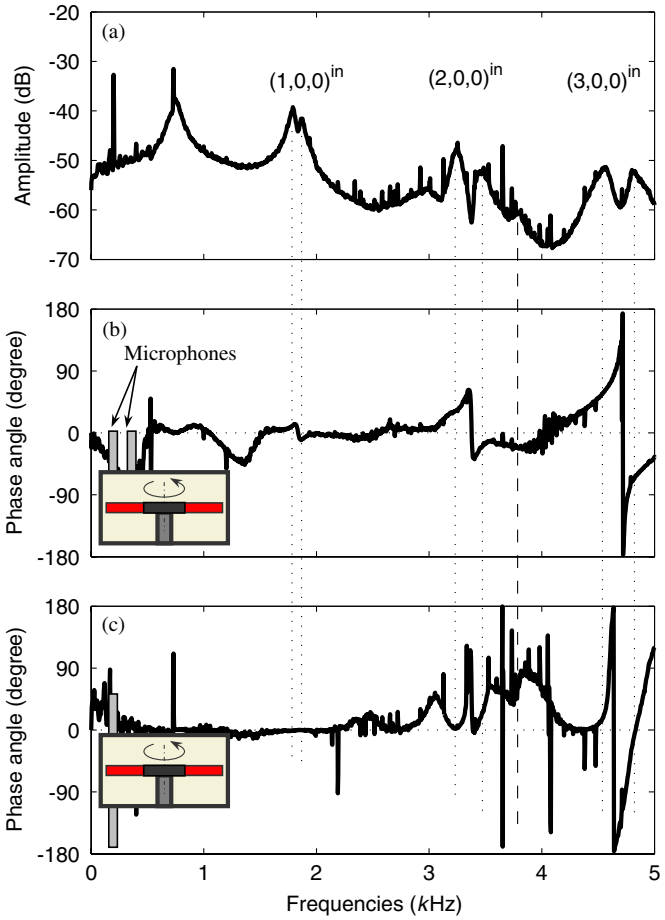

Fig. 5. Spectra of acoustic pressures oscillations in a cylindrical enclosure when an aluminum disk (0.005″ thick) is rotating at 12×10^3 rev/min in the middle of the enclosure: (a) auto-power spectrum, (b) cross-power spectrum between top 1 and 2, and (c) cross-power spectrum between top and bottom.

3.2. Disk vibrations

The transverse vibrations of the rotating disks in the cylindrical enclosure are also measured simultaneously with the acoustic pressure. In this measurement, no speaker is used, so that fluid unsteadiness alone excites disk vibrations. Measurements are performed in the vicinity of the OD (outer radius) position of the disks, when the disks rotate in the range of 4–23 $\times 10^3$ rev/min at intervals of 250 rev/min without any intentional external excitation.

Fig. 6(a) shows the waterfall plot of the power spectral density of transverse vibrations of a very thin plastic disk (0.005″ thick). In this experiment, several reflected traveling waves at super-critical speed are excited by air turbulence. Two, three and four nodal diameter modes become reflected traveling waves above 4×10^3 rev/min, which is the lowest rotating speed of this experiment. For comparison, the coupled natural frequencies of the rotating disk in the enclosure are also computed in Fig. 6(b), using the developed model [11]. Identical dimensions of the enclosure and disk are used for the computation. Further, material properties in Table 2 and 30% bulk rotating flow ($\Omega_f = 30\%\ \Omega_d$) are used for the computation. Overall trends of the computational results agree well with experimental ones. However, because the higher nodal circle modes tend to be excited by turbulence only at much higher speed, it is not easy to correlate all the experimentally observed vibration modes with those in the computation.

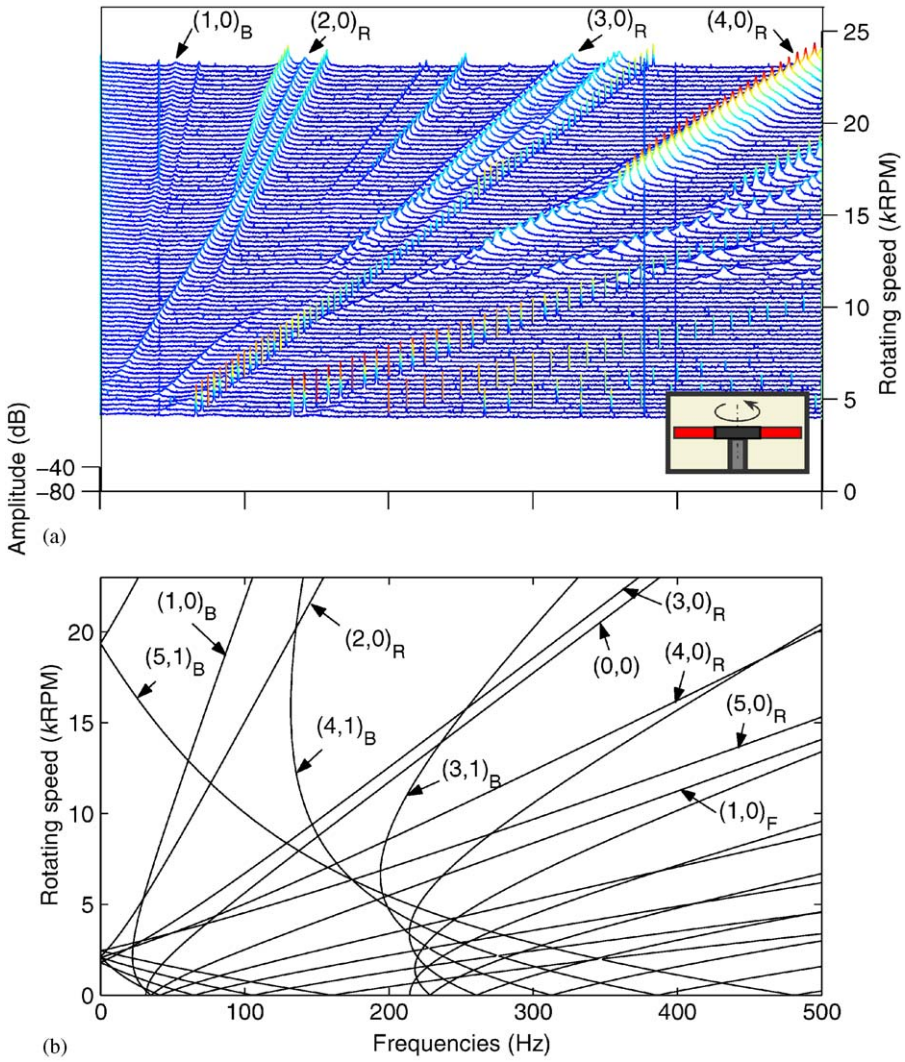

Fig. 6. Transverse vibrations of a rotating disk in the enclosure (plastic disk, 0.005″ thick): (a) experimental results, and (b) computational results including acoustic–structure coupling.

Note that the disk runout components generally decrease with increasing rotation speeds, because the rotational stresses tend to reduce the slight natural out-of-plane warping of the disk. To identify the vibration modes, the phase angle of the cross-power spectrum between two signals measured by laser sensors through the top cover are also calculated applying the same technique as before for the acoustic modes. For instance, Fig. 7 shows auto-power and cross-power spectra of the plastic disk (0.005″ thick) rotating at 15×10^3 rev/min. At the frequencies of the peaks in the auto-power spectrum, phase angles of cross-power spectrum agree well with the number of nodal mode diameter, times the angular separation of two laser sensors (about 25° in this experiment). Note that because two laser sensors are installed along the circumferential direction, the technique of this analysis is capable of identifying only the nodal diameter of the modes and not the nodal circle. Nodal circle modes however are not detected in this experiment. The two peaks in Fig. 7 near 105 and 210 Hz have somewhat different characteristics and will be discussed in the next section.

As the speed of the plastic disk is increased further ($\sim 16 \times 10^3$ rev/min) beyond its critical speed, the amplitude of the (4,0) disk mode increases suddenly (see Fig. 6(a)). This phenomenon is called the *flutter instability* and the corresponding rotating speed is called the *flutter speed*. However, it is difficult to quantify

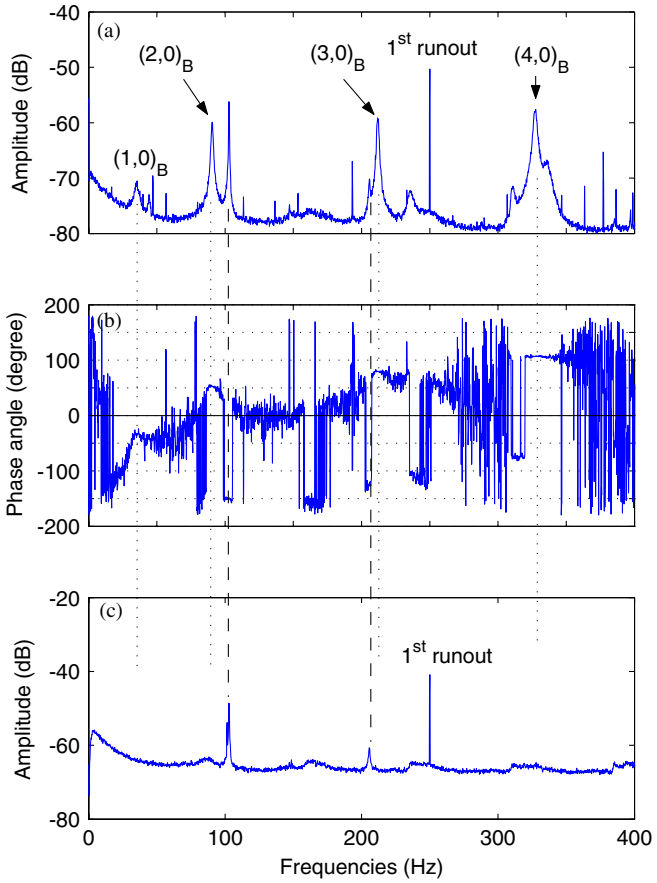

Fig. 7. Auto- and cross-power spectra of a flexible disk rotating at 15×10^3 rev/min (below flutter speed) in a cylindrical enclosure (plastic disk, 0.005″ thick): (a) auto-power spectrum of the rotating disk, (b) phase angle of cross-power spectrum of the rotating disk, and (c) auto-power spectrum of acoustic pressure in an enclosure.

precisely the flutter speed in an experiment. There have been several attempts to define the flutter speeds of rotating disks more precisely in experiments. For example, Renshaw et al. [6] defined flutter speed as the rotation speed at which a vibration frequency peak reached at least 20 dB above the noise level, whereas Hansen et al. [7] defined it based on the intersection of a wave speed curve and a corresponding damping speed curve. However, the first is somewhat *ad hoc*, and the second requires precise experimental technique to extract disk dampings of forward and backward traveling waves. For these reasons, in this experiment the flutter speed is approximated from the amplitude variation as a function of speed, as shown in Fig. 8. The amplitudes of (4,0) BTW beyond 15.5×10^3 rev/min much larger than those at lower speeds. The vibration amplitude grows up to 18 *k*RPM, and is likely to be limited by disk and fluid nonlinearities. Interestingly, beyond the flutter speed at 16×10^3 rev/min, the (2,0) BTW mode splits into two frequency peaks. This phenomenon is similar as that observed by Lee et al. [14].

Besides the flutter speed, it is also interesting to measure acoustic–structure coupling in the post-flutter region. As shown in Fig. 9, near 490 Hz, the (4,0) BTW mode flutters, and the amplitude of the auto-power spectrum of the acoustic pressure oscillation at the corresponding frequency also becomes very large. In the pre-flutter region, the acoustic pressure is insignificant at any disk mode frequency (compare Fig. 9 with Fig. 7). From this observation, it can be deduced that the acoustic–structure coupling becomes significant when the disk becomes unstable.

Finally, considering the mechanism of the instability described in the accompanying paper, it is clear that the flutter instability observed in this experiment is not from mode coalescence. It is a damping-induced instability because a single reflected traveling wave ((4,0) RTW) becomes unstable at the flutter speed.

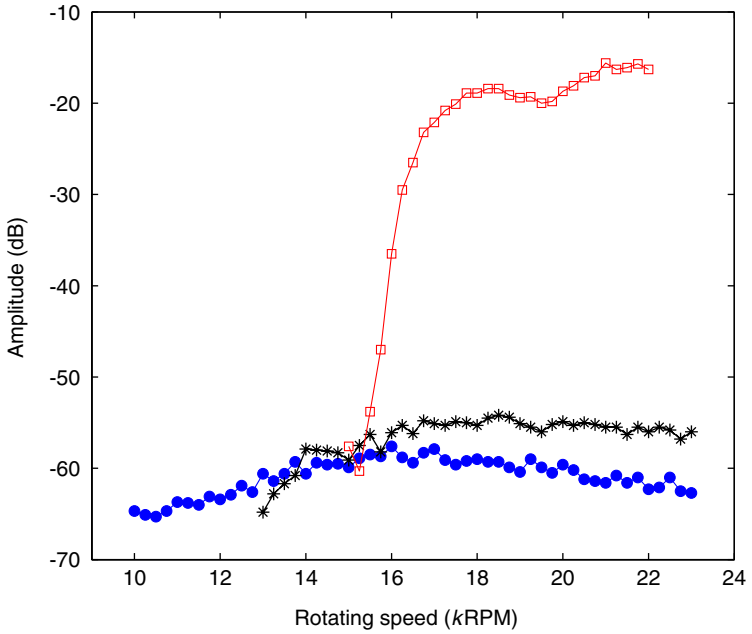

Fig. 8. The amplitude of three vibration modes as a function of rotating speed (plastic disk, 0.005″ thick): ●, $(2,0)_R$; ∗, $(3,0)_R$; □, $(4,0)_R$.

In general there exist three kinds of dampings (disk, acoustic and fluid viscous dampings) in the real system. Therefore, to predict precisely the flutter speed, it is necessary to know accurately all the damping values in the theoretical model. However, the determination of damping needs more elaborate experiments, and is still an ongoing research topic.

3.3. Subharmonics at half rotation speed

While measuring disk and acoustic oscillations, several other interesting phenomena are also observed in this experiment. For example, the origin of two peaks near 105 and 210 Hz in Fig. 7 is not explained yet. The shapes of the peaks are sharp like those of disk runout. Interestingly, these modes seem to evolve from near-zero frequency when the disk is at rest. In addition, those peaks exist irrespective of the different disk material used (compare Fig. 10(a) with Fig. 6(a)). Moreover, these peaks are not present when the top cover of the enclosure is removed, as shown in Fig. 10(b). Therefore, it can be concluded that these peaks are not caused by disk characteristics such as imperfection or unbalance of the disk. Another observation of the unknown peaks is also illustrated in the auto-power spectrum of acoustic pressure oscillation. As shown in Figs. 7 and 9, the amplitudes of acoustic pressure at the frequencies corresponding to the peaks in the auto-power spectrum are quite significant. Although the amplitudes of the unknown peaks are smaller than those of disk modes in the auto-power spectrum of the disk, the microphone on the top cover detects only the components of unknown peaks. Therefore, it is almost certain that these peaks are caused by unsteadiness in the airflow of the surrounding fluid, and seem to be related to fluid rotation.

Interestingly, the frequency of the first peak is almost half the frequency of disk rotation, which is close to the frequency of the rotating fluid speed reported in several publications [15,16]. While this phenomenon may also resemble oil *whirl* instability [17,18], this resemblance is entirely coincidental. The exact mechanisms of the subharmonic peaks observed in this work, therefore, are still unknown and are to be studied in the future.

3.4. Effects of presence or absence of top cover

Experiments are also performed on the self-excited disk oscillations to understand the effects of the top cover using a 0.01″ thick plastic disk (Fig. 10). In the absence of the top cover (Fig. 10(b)), the flutter

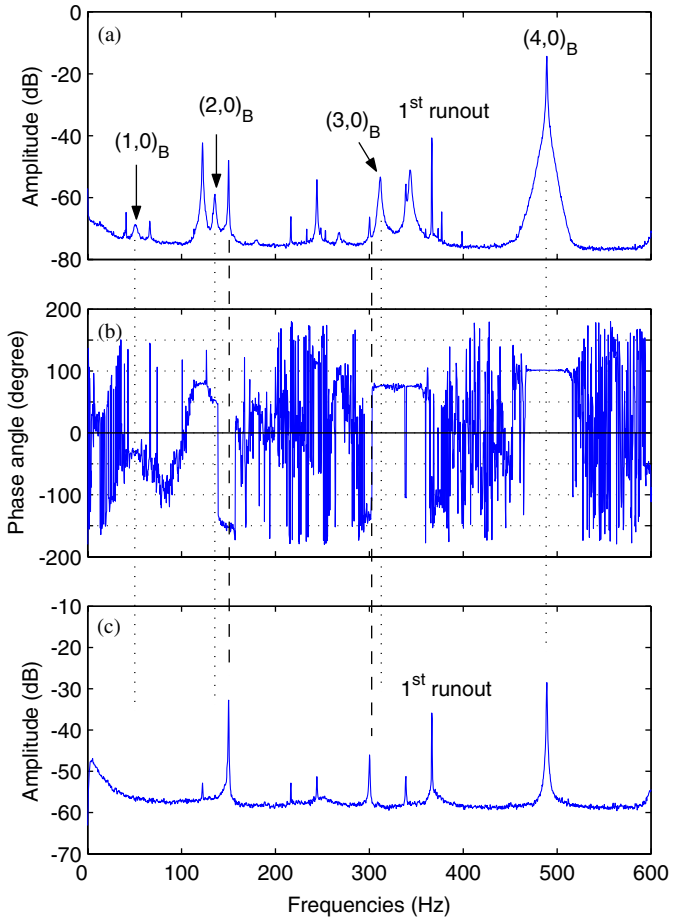

Fig. 9. Auto- and cross-power spectra of a flexible disk rotating at 22×10^3 rev/min (above flutter speed) in a cylindrical enclosure (plastic disk, 0.005″ thick): (a) auto-power spectrum of the rotating disk, (b) phase angle of cross-power spectrum of the rotating disk, and (c) auto-power spectrum of acoustic pressure in an enclosure.

instability of the (3,0) mode is observed near 13×10^3 rev/min and the rate of change of disk frequencies with respect to the rotating speed changed suddenly at this speed. However the frequencies beyond flutter speed do not lock completely onto a constant frequency. When D'Angelo and Mote first observed the frequency lock-on phenomenon, the disk was rotated in an unbounded domain [5]. Therefore fluid boundary conditions may cause differences in frequency lock-on behaviors in the post-flutter region. On the other hand, the frequency lock-on phenomenon is not observed in the presence of the top cover. Clearly these results suggest a strong influence of enclosure boundary conditions on post-flutter dynamics.

4. Discussion and conclusions

The vibrations and instability of a rotating disk coupled to acoustic oscillations of surrounding air are investigated experimentally. From the acoustic pressure measurement, it is shown that the in-phase and out-of-phase acoustic modes exist in the enclosure. Further, the acoustic modes split into forward and backward traveling waves, as the disk rotates. The amount of acoustic mode split enables the estimation of rotating speed of the surrounding fluid in the enclosure. From the vibration measurement of the rotating disk, flutter instability of RTW is observed at supercritical speeds. Beyond the flutter speed, it is also observed that acoustic pressures oscillate severely at the frequency of disk instability. The flutter instability observed in this experiment is not the mode coalescence but a damping-induced instability leading to the flutter of a single

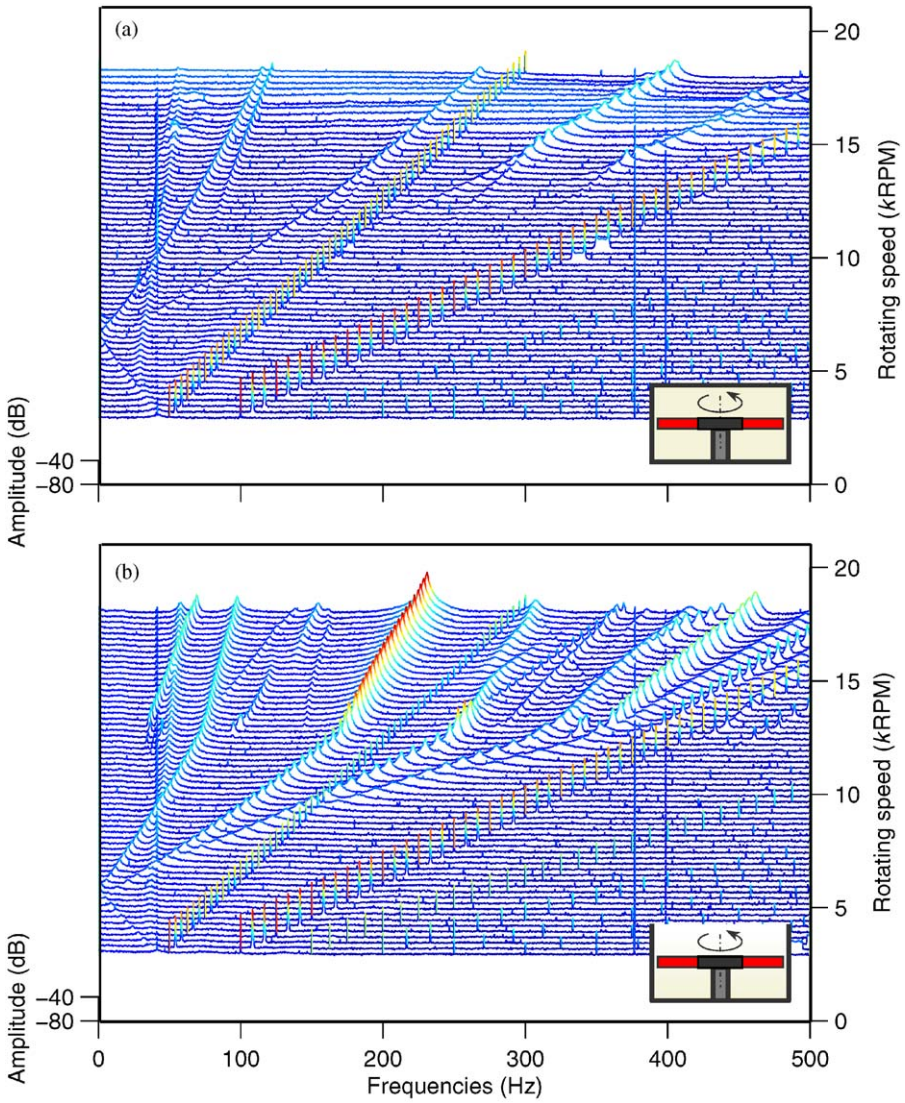

Fig. 10. Waterfall plot of transverse vibrations of a rotating disk in the enclosure (plastic disk, 0.01″ thick): (a) with top cover, and (b) without top cover.

reflected traveling wave. These experimental observations agree well with theoretical predictions, which are proposed in the accompanying paper.

However, experiments also show some phenomena which are not predicted by the proposed model. For example, disk flutter speeds in theoretical prediction and experimental measurement are not directly compared in this study. In order to predict the flutter speed accurately, accurate values of damping are necessary. Indeed, the stability of the acoustic–structure coupled system is determined by the interplay of disk, acoustic and fluid dampings, and therefore all the damping values should be determined prior to the prediction of flutter speed. Clearly, future experiments will need to measure accurately the disk, acoustic, and fluid damping in order to provide better system parameters that can then be used to close the gap between the theoretically predicted and experimentally measured flutter speeds and modes. To determine disk damping, initial experiments will need to be performed in vacuum. To determine acoustic damping, the disk can be replaced by a much stiffer material, so that the disk modal structure moves into a very high frequency regime and does not interact with the acoustic modes. Acoustic excitation using speakers along the lines of what is shown in the paper would

then in principle lead to accurate estimates of the acoustic damping at different rotation speeds. With knowledge of the disk material damping, the acoustic damping as a function of speed, and the angular speed of the rotating potential core, it should be possible in principle to measure the effective viscous damping as a function of speed.

Finally, the proposed theory needs to be updated to predict observed nonlinear phenomena such as the subharmonics at half-disk rotation speed and post-flutter dynamics. It is likely that such models will need to include both structural and fluidic nonlinearities and are the subject of ongoing research.

Acknowledgements

The authors thank the Purdue Research Foundation, Seagate Technology, and the National Science Foundation (NSF) for financial support provided under Award (CAREER) 0134455-CMS. The authors would also like to thank Professors J.S. Bolton and A.K. Bajaj (Purdue University) and S. Tadepalli (Seagate Technology) for fruitful discussion during the course of this research.

References

[1] J.S. McAllister, The effect of disk platter resonances on track misregistration in 3.5 inch disk drives, *IEEE Transactions on Magnetics* 32 (3) (1996) 1762–1766.
[2] S. Imai, M. Tokuyama, Y. Yamaguchi, Reduction of disk flutter by decreasing disk-to-shroud spacing, *IEEE Transactions on Magnetics* 35 (5) (1999) 2301–2303.
[3] S. Imai, Fluid dynamics mechanism of disk flutter by measuring the pressure between disks, *IEEE Transactions on Magnetics* 37 (2) (2001) 837–841.
[4] G. Bouchard, F.E. Talke, Non-repeatable flutter of magnetic recording disks, *IEEE Transactions on Magnetics* 22 (5) (1986) 1019–1021.
[5] C. D'Angelo, C.D. Mote Jr., Aerodynamically excited vibration and flutter of a thin disk rotating at supercritical speed, *Journal of Sound and Vibration* 168 (1) (1993) 15–30.
[6] A.A. Renshaw, C. D'Angelo, C.D. Mote Jr., Aeroelastically excited vibration of a rotating disk, *Journal of Sound and Vibration* 177 (5) (1994) 577–590.
[7] M. Hansen, A. Raman, C.D. Mote Jr., Estimation of nonconservative aerodynamic pressure leading to flutter of spinning disks, *Journal of Fluids and Structures* 15 (2001) 39–57.
[8] B.C. Kim, A. Raman, C.D. Mote Jr., Prediction of aeroelastic flutter in a hard disk drive, *Journal of Sound and Vibration* 238 (2) (2000) 309–325.
[9] J.G. Tseng, J.A. Wickert, Split vibration modes in acoustically-coupled disk stacks, *ASME Journal of Vibration and Acoustics* 120 (1998) 234–239.
[10] J.S. Park, I.Y. Shen, Aerodynamically and structurally coupled vibration of multiple co-rotating disks, *ASME Journal of Vibration and Acoustics* 126 (2004) 220–228.
[11] N. Kang, A. Raman, Vibration and stability of a flexible disk rotating in a gas filled enclosure—part I: theoretical study, *Journal of Sound and Vibration*, this issue (doi:10.1016/j.jsv.2005.09.001).
[12] C. D'Angelo, C.D. Mote Jr., Natural frequencies of a thin disk clamped by thick collars with friction at the contacting surfaces spinning at high rotating speed, *Journal of Sound and Vibration* 168 (1) (1993) 1–14.
[13] T.K. Ahn, C.D. Mote Jr., Mode identification of a rotating disk, *Experimental Mechanics* 38 (4) (1998) 250–254.
[14] S.Y. Lee, J.D. Kim, S. Kim, Critical and flutter speeds of optical disks, *Microsystem Technologies* 8 (2002) 206–211.
[15] C.A. Schuler, W. Usry, B. Weber, J.A.C. Humphrey, R. Greif, On the flow in the unobstructed space between shrouded corotating disks, *Physics of Fluids* A2 (10) (1990) 1760–1770.
[16] D. Dijkstra, G.J.F. Van Heijist, The flow between two finite rotating disks enclosed by a cylinder, *Journal of Fluid Mechanics* 128 (1983) 123–154.
[17] A. Muszynska, Whirl and whip—rotor/bearing stability problems, *Journal of Sound and Vibration* 110 (3) (1986) 443–462.
[18] T. Jintanawan, I.Y. Shen, K. Tanaka, Vibration analysis of fluid dynamic bearing spindles with rotating-shaft design, *IEEE Transactions on Magnetics* 37 (2) (2001) 799–804.